frontiers in Chemistry

ORIGINAL RESEARCH
published: 01 October 2019
doi: 10.3389/fchem.2019.00649

Synthesis of Flower-Like g-C_3N_4/BiOBr and Enhancement of the Activity for the Degradation of Bisphenol A Under Visible Light Irradiation

Jun Wu[1], *Yu Xie*[1]*, *Yun Ling*[1], *Yunyun Dong*[2], *Jian Li*[1], *Shiqian Li*[1] and *Jinsheng Zhao*[2]*

[1] College of Environment and Chemical Engineering, Nanchang Hangkong University, Nanchang, China, [2] College of Chemistry and Chemical Engineering, Liaocheng University, Liaocheng, China

The high recombination rates of photogenerated electron-holes greatly inhibit the catalytic activity of semiconductor photocatalysts. Herein, the heterojunctions of the flower-like g-C_3N_4/BiOBr composites were synthesized as photocatalysts by a simple hydrothermal process. The X-ray diffraction, scanning electron microscopy, and X-ray photoelectron spectrometer were utilized to characterize the sample's structure and light absorption properties. The results demonstrated that BiOBr-g-C_3N_4-4:1 showed excellent photocatalytic properties and 96.6% of bisphenol (BPA) was removed in 120 min with illumination of visible light due to its narrower band gap than that of pure BiOBr. BiOBr offer little electrons during the photocatalytic reaction. Moreover, the heterostructure between BiOBr and g-C_3N_4 facilitates the separation of photogenerated carriers. Excellent stability was exhibited after five cyclic degradation of methyl orange (MO) with the illumination of visible light. The active species trapping experiment indicated that superoxide radical anions ($O_2^{\bullet-}$) and hole (h^+) have a great effect on the reaction. A possible mechanism was proposed to explain the whole process of photocatalytic reaction.

Keywords: BiOBr, g-C_3N_4, photocatalysts, heterojunctions, pollutant degradation

OPEN ACCESS

Edited by:
Zhenhai Wen,
Chinese Academy of Sciences, China

Reviewed by:
Shun Mao,
Tongji University, China
Yihe Zhang,
China University of Geosciences, China

***Correspondence:**
Yu Xie
xieyu_121@163.com
Jinsheng Zhao
j.s.zhao@163.com

Specialty section:
This article was submitted to Catalysis and Photocatalysis, a section of the journal Frontiers in Chemistry

Received: *29 May 2019*
Accepted: *10 September 2019*
Published: *01 October 2019*

Citation:
Wu J, Xie Y, Ling Y, Dong Y, Li J, Li S and Zhao J (2019) Synthesis of Flower-Like g-C_3N_4/BiOBr and Enhancement of the Activity for the Degradation of Bisphenol A Under Visible Light Irradiation. Front. Chem. 7:649. doi: 10.3389/fchem.2019.00649

HIGHLIGHTS

- Flower-like g-C_3N_4/BiOBr nanosheets were prepared by a facile hydrothermal method.
- The red-shift of the absorption peak of BiOBr-g-C_3N_4 composite was observed.
- The BiOBr-g-C_3N_4-4:1 exhibited the highest photocatalytic performance.

INTRODUCTION

Bisphenol A (BPA) is named as 2,2-(4,4-dihydroxydiphenyl) propane, and can be synthesized from phenol and acetone in an acidic medium, which is an important raw material for epoxy resin, polycarbonate, polysulfone, polyarylate, and other products (Tsai, 2006). A primary problem of this material is that upon the release of BPA into the environment, it needs to be degraded in order to become a harmless substance.

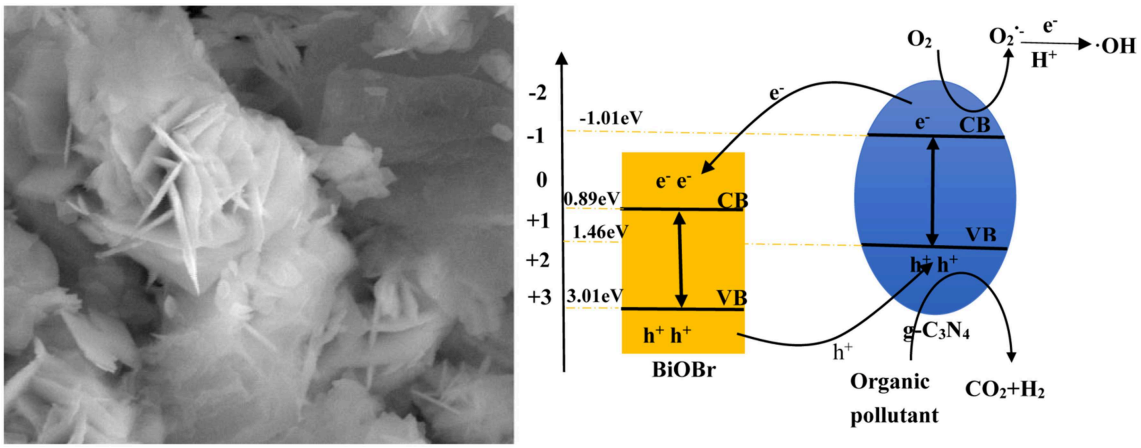

GRAPHICAL ABSTRACT | The flower-like BiOBr-g-C3N4 nanosheet and possible mechanism for BPA degradation.

Several biotic and abiotic methods have been proposed to degrade BPA in wastewater. For example, the ready biodegradability of BPA was evaluated by Athanasios S. Stasinakis by using activated sludge as inoculum with the OECD method 301F (manometric respirometry test) that measures O_2 production (Stasinakis et al., 2008). In the meantime, a lot of abiotic methods (chemical and physical methods) have been reported. Wu reported BPA degradation by means of releasing nano-TiO_2 into a water environment with BPA at low concentration (Wu et al., 2016). It was proved that the abiotic degradation rate of BPA was significantly facilitated with the illumination of light. However, at present, both biodegradation and non-biological reduction have the disadvantages of low efficiency and cumbersome. In order to solve the problem, the artificial photocatalytic process furnishes a viable strategy and aroused great interest among researchers (Sun et al., 2017; Liu et al., 2019).

In 1972, the TiO_2 electrode was employed for the decomposition of water to produce hydrogen and oxygen by Fujishima and Honda (1972), which opened up a new era of researchers looking for semiconductor photocatalysts (Maeda et al., 2006). Nevertheless, on the one hand TiO_2 just works on the radiation of ultraviolet light because of its wide band gap and ultraviolet light only accounts for ∼5% of sunlight (Fu et al., 2012). On the other hand, the large band-gap oxide semiconductor has short exciton diffusion lengths when TiO_2 is applied in photoelectrochemical devices. Therefore, it is mainly the carriers generated in the space charge layer that contribute to the photocurrent (Santato et al., 2001). A novel semiconductor photocatalyst was investigated to be an alternative to TiO_2-based materials (Zou et al., 2001; Osterloh, 2008). A polymeric graphitic carbon nitride (g-C_3N_4) aroused great interest in the field of semiconductor photocatalysts (Wang and Antonietti, 2012). A metal-free catalyst that contains carbon and nitrogen elements and a small amount of hydrogen, it has a narrow band gap which has a wide visible light absorption rage in the visible region, and high thermal and chemical stability thanks to its tri-s-triazine ring (Wang and Antonietti, 2012; Chen et al., 2014; Zhou et al., 2014). However, pure g-C_3N_4 has poor photocatalytic performance regarding limited organic pollutants due to its low quantum efficiency, which limits its practical applications (Liu et al., 2010; Yan et al., 2010). So far, great efforts have been taken to improve the photocatalytic performance of g-C_3N_4, such as metal and nonmetal elements doping (Zhang et al., 2009; Liu et al., 2010; Wang et al., 2010), designing different morphology (Groenewolt and Antonietti, 2005; Vinu et al., 2005; Goettmann et al., 2006; Lu et al., 2014), constructing heterostructure with other semiconductor photocatalysts such as ZnO (Kuang et al., 2015), Cu_2O (Peng et al., 2014), MoS_2 (Li et al., 2014), Fe_3O_4 (Chi et al., 2016), Bi_2WO_6 (Wang et al., 2017). Actually, modified g-C_3N_4 shows excellent photocatalytic properties because the modification of g-C_3N_4 with other photocatalysts promotes the separation of photogenerated carries.

Recently, it was reported that bismuth oxyhalides is a new family of photocatalysts, which showed broad application prospects in the photocatalytic degradation of organic pollutants due to its unique and intrinsic lamellar structures structure as well as the appropriate bandgaps (tetragonal matlockite structure) (Zhang et al., 2006, 2008; Huang et al., 2017a). The structure of the indirect-transition band gap makes the excited electrons emit to the valence band (VB) at a certain K-space distance, thus prolonging the lifetime of the photogenerated carries (Zhang et al., 2006; Chen et al., 2019). In addition, the structures of the [Bi_2O_2] plate are interlaced by double slabs of halogen atoms, which provide enough room to polarize the related kernel and orbital. As a resultant, the internal static electrostatic area is perpendicular to the [Bi_2O_2] slabs and halogen anionic slabs in BiOX (Zhang et al., 2006; Huang and Zhu, 2008; Ye et al., 2011; Jiang et al., 2012a). Moreover, BiOX exhibited superior practical application in pigments (Maile et al., 2005), catalysts (Kijima et al., 2001), storage materials and ferroelectric materials (Kusainova et al., 2001; Lei et al., 2010). In particular, there is much research on the photocatalytic performance of BiOBr. For instance, Shang's group reported the preparation of a pure BiOBr catalyst with lamellar structure, which was synthesized by hydrothermal method using cetyltrimethylammonium bromide (CTAB) as

Bromine source and template and its photocatalytic activity is four times higher than that of its analog made from KBr as the Br source (Shang et al., 2009). Kong's group designed and prepared AgBr-BiOBr heterojunction photocatalysts by varying the loadings of AgBr by an effective co-precipitation method and the obtained catalyst displayed excellent photocatalytic performance on the degradation of Rhodamine B (RhB) under visible-light irradiation (Kong et al., 2012). Thence, there is still a long way to go to find more ways for the preparation of doped BiOBr as photocatalysts.

Herein, we report that a flower-like nanoflake BiOBr-g-C_3N_4 with high photocatalytic activity was synthesized by a simple one step hydrothermal method. The CTAB was applied as Br source and template. The catalytic activity of the prepared samples of BiOBr-g-C_3N_4 were surveyed by the degradation of BPA in visible light (lambda > 420 nm). A 300W Xe lamp was used as light source with ultraviolet light absorbed by filter. The structure and optical properties were characterized by SEM, TEM, XRD, XPS. The result demonstrated that BiOBr-g-C_3N_4 heterojunctions were successfully prepared and a possible mechanism of photocatalytic degradation was proposed. The heterojunction exhibited higher photocatalytic activity than that of pure BiOBr or g-C_3N_4. Besides, the flower-like structure was synthesized by controlling experimental condition.

EXPERIMENTAL

Photocatalytic Preparation

Materials

Melamine was bought form Sinopharm Chemical Reagent Co., Ltd. Ethylene glycol and bismuth nitrate pentahydrate [$Bi(NO_3)_3{\cdot}5H_2O$] was purchased from Xilong Chemical Co., Ltd. CTAB was acquired from Shanghai Zhanyun Chemical Co., Ltd. All reagents are analytical pure on this work.

Preparation of Bulk g-C_3N_4

The bulk g-C_3N_4 nanoplates were made according to previous report (Liang and Zhu, 2016). 2 g of melamine was added to the porcelain crucibles with a cover. And then, the crucibles were moved to a Muffle furnace and heated to 550°C for 4 h at a heating rate of 5°C min^{-1}. The product is claimed and cooled to room temperature. Collecting the yellow products and grinding it into powder for further use.

Preparation of BiOBr-g-C_3N_4 Photocatalysts

BiOBr-g-C_3N_4 photocatalysts were synthesized by a sample hydrothermal method with different ratio. To begin with, measured a certain amount of CTAB and the as prepared g-C_3N_4 were added into 16 ml of ethylene glycol and the mixture was stirred vigorously for 30 min to obtain a uniform suspension at room temperature. Meantime, A certain amount of $Bi(NO_3)_3{\cdot}5H_2O$ solid was dissolved in 12 ml of nitric acid solution and be stirred for another 30 min to obtain a clear solution. Subsequently, the solution was poured rapidly into the suspension and the mixture was ultrasonicated for another 30 min at room temperature. The obtained mixture was moved to 50 ml Teflon-lined autoclave. Afterward, the autoclave was heated in a constant temperature drying box, and the temperature was kept at 160°C for 12 h. And then, the autoclave was cooled to room temperature after thermal polycondensation. The precipitation was obtained by centrifugation. The precipitation was washed with deionized water and absolute ethanol for three times, respectively. The samples were transferred to oven to dry at 80°C for all night. As a result, different mass ratios of samples were named BiOBr-g-C_3N_4-a:b (a:b = 8:1, 4:1, 1:1, 1:4, where a:b was the mass ratios of BiOBr to g-C_3N_4, respectively). Otherwise, it was worth noting that the quantity of BiOBr was obtained by measuring raw materials of $Bi(NO_3)_3{\cdot}5H_2O$ and CTAB.

Characterization

The X-ray diffraction (XRD) pattern of the samples were measured by RiGdku RINT 2000 X-ray diffractometer (λ = 1.5418Å) with a CuKα radiation source. Scanning electron microscope (SEM) was used for observing the structure of pure BiOBr and BiOBr-g-C_3N_4 composites. The optical properties for samples were detected by Spec-3700 DUV Shimadzu UV-visible spectrophotometer. The elemental composition and chemical states were measured by X-ray photo-electron spectroscopy (XPS). The amount of BPA in the aqueous solution was measured by the use of a high-performance liquid chromatograph (HPLC, Agilent 1260), equipped with a photo diode array detector (PDAD) and a ZORBAX Eclipse XDB-C18 column.

Photocatalytic Activity Test

The catalytic activities of samples were assessed with photocatalytic degradation of Bisphenol A (BPA) under the illumination of visible light. For the visible-light photocatalytic study, a 300W Xe lamp (PLS-SXE300, Beijing, Perfectlight Technology Co., Ltd.) was used as the visible light source with a 420 nm cutoff filter. In each experiment, 10 mg of catalyst power was added into the BPA solution (50 ml, 10 mg L^{-1}) by continuous stirring at normal atmospheric temperature. Prior to the irradiation, the suspension was magnetically stirred in dark for 30 min to establish adsorption-desorption equilibrium. In given time intervals, collecting 3 mL of supernatant and the catalyst particles were removed by centrifugation. The content of the BPA in the supernatant was analyzed by HPLC.

Photocurrent Tests

The separation efficiency of photogenerated electron-hole pairs was recorded on CHI660D electrochemical workstation by using a standard three-electrode system. Saturated sodium sulfate solution was used as electrolyte. The graphite electrode and Ag/AgCl electrode was selected as counter electrode and reference electrode, and the samples derived electrodes were served as the working electrode. A 300W Xe lamp (PLS-SXE300, Perfectlight Company, Beijing, China) of 100 mW/cm^2 UV-Vis light intensity was employed as light source. For preparing the working electrodes, 10 mg of sample was dispersed in 1 mL of absolute ethanol to obtain suspension, and the suspension was ultrasonicated for 10 min. The slurry was dipped and coated on the surface of fluorine-tin oxide (FTO) glass substrates, which was dried at room temperature overnight.

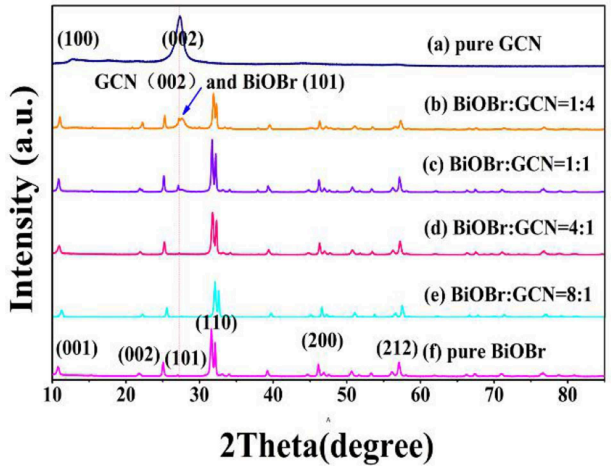

FIGURE 1 | XRD pattern of BiOBr-g-C_3N_4 composites, pure BiOBr and g-C_3N_4.

RESULTS AND DISCUSSION

Crystal Phase and Morphology Characterization

Figure 1 represents the X-ray pattern of the BiOBr-g-C_3N_4 composites, and the patterns of pure g-C_3N_4 and pure BiOBr. The g-C_3N_4 exhibits two different diffraction peaks. The high-intensity peak at 26.50° was related to (002) crystal plane of g-C_3N_4, attributing to the accumulation of aromatic segments, and the low-peak at 13.028° was related to (100) crystal plane, corresponding to the in-plane structural filling order (JCPDS 87-1526). The result was consistent with previous reports (Yan, 2012; Chang et al., 2013; Hao et al., 2019). The X-ray diffraction peaks of pure BiOBr at 10.907°, 21.914°, 32.241°, 46.241°, and 57.162° were corresponded to (001), (002), (110), (200), and (212) crystal plane of BiOBr, respectively, which can correspond to tetragonal BiOBr (JCPDS 09-0393). All peaks of BiOBr could be found in the patterns of pure BiOBr and BiOBr-g-C_3N_4 composites and no other impurity peaks can be observed, which indicates that BiOBr and g-C_3N_4 composites were successfully synthesized by a hydrothermal method. The diffraction peak of the (001) plane of BiOBr-g-C_3N_4 was shifted to an higher diffraction angle, indicating the interaction between BiOBr and g-C_3N_4 contributes to the formation of BiOBr-g-C_3N_4 heterojunction (Ye et al., 2013; Yang et al., 2017; Zhang et al., 2019). Otherwise, the sharp diffraction peak of the BiOBr stage display that BiOBr has high crystallinity in this heterojunction. No significant change in the position of the diffraction peak was observed in BiOBr-g-C_3N_4 composites, implying that the size and structure of the photocatalysts were not destroyed.

The surface morphology and structure of pure BiOBr and BiOBr-g-C_3N_4-4:1 heterojunction was exhibited in **Figure 2**. As can be seen in **Figure 2a**, the pure BiOBr exhibit a regular shape that look like flower, and it is self-assemble from many conventional biological sheets with the thickness of about 30–50 nm. Each large nanosheet is formed from a stack of many thin nanosheets. **Figure 2b** shows the morphology of BiOBr-g-C_3N_4-4:1 composite, the g-C_3N_4 and BiOBr nanoflakes could be observed. Unlike the pure flower-like BiOBr nanoflake, the nanoflake structure of BiOBr was destroyed, and be interwoven with g-C_3N_4 in the BiOBr-g-C_3N_4 composite. In other words, the introduction of g-C_3N_4 inhibits the assembly of BiOBr. However, it could provide a number of nucleation sites for the reaction because of its abundant surface functional groups of g-C_3N_4 (Di et al., 2015). The bulk g-C_3N_4 was formed on the surface of BiOBr, which was propitious to form BiOBr-g-C_3N_4 heterojunction from the close contact between these two components. The C, N, Bi, O, Br elements were present in BiOBr-g-C_3N_4-4:1 composite according to the EDS spectra in **Figures 2c–g**. Meantime, performing elemental mapping measurements to further determine the presence and distribution of C, N, Bi, O, Br elements, indicating that the BiOBr nanosheets were deposited successfully on the surface of g-C_3N_4 and the BiOBr-g-C_3N_4 heterojunctions were synthesized successfully. The result is in accordance with the result observed from the XRD patterns.

Band Gap and Chemical State Analysis

The elemental composition and chemical states were recorded on X-ray photoelectron spectroscopy. The C, N, Bi, O, Br elements were observed according to the XPS survey scan spectrum shown in **Figure 3A**, further revealing that BiOBr-g-C_3N_4 heterojunctions were synthesized successfully, which were consistent with the above-mentioned EDS patterns. The spectrum of Br 3d was shown in **Figure 3B**, and two typical peaks at about 68.0 and 69.0 eV were observed and attributed to $Br3d_{5/2}$ and $Br3d_{3/2}$ of Br- in BiOBr-g-C_3N_4 composites or pure BiOBr (Cheng et al., 2011; Huo et al., 2012; Liu et al., 2014). No obvious movement in the position of the Br3d peak was observed in **Figure 3B**, indicating that there is no influence on the energy spectrum of Br by coupling with g-C_3N_4 (Wang et al., 2015). As is displayed in **Figure 3C**, the two peaks at 159 and 164.3 eV belonged to Bi $4f_{5/2}$ and Bi $4f_{7/2}$, respectively, corresponding to the Bi element in trivalent oxidation state. It is noted that the two peaks of Bi 4f have a slight shift to low binding energy of 158.9 and 164.2 eV, which may be due to the connection between BiOBr and g-C_3N_4 (Fu et al., 2012; Huang et al., 2017b). For O 1s spectrum of pure BiOBr and BiOBr-g-C_3N_4 composites **Figure 3D**, the peak with binding energy at 532.1 eV was converted to low binding energy at 532.0 eV. However, no significant effects were observed in the position of the binding energy at 529.6 eV. The peak at 529.6 eV was corresponding to crystal lattice O atoms (Bi-O) and the peak at 532.0 eV was attached into O-H which is derived from surface absorption of photocatalysts (Huo et al., 2012; Zhu et al., 2012; Liu et al., 2014). The analysis result indicated the formation of the BiOBr-g-C_3N_4 heterojunction (Zhang et al., 2019).

Electronic Transfer Path Analysis

The electronic transfer path of pure BiOBr, pure g-C_3N_4, and BiOBr-g-C_3N_4 composites were measured with UV-vis diffuse reflectance spectra (DRS). The fundamental absorption edges

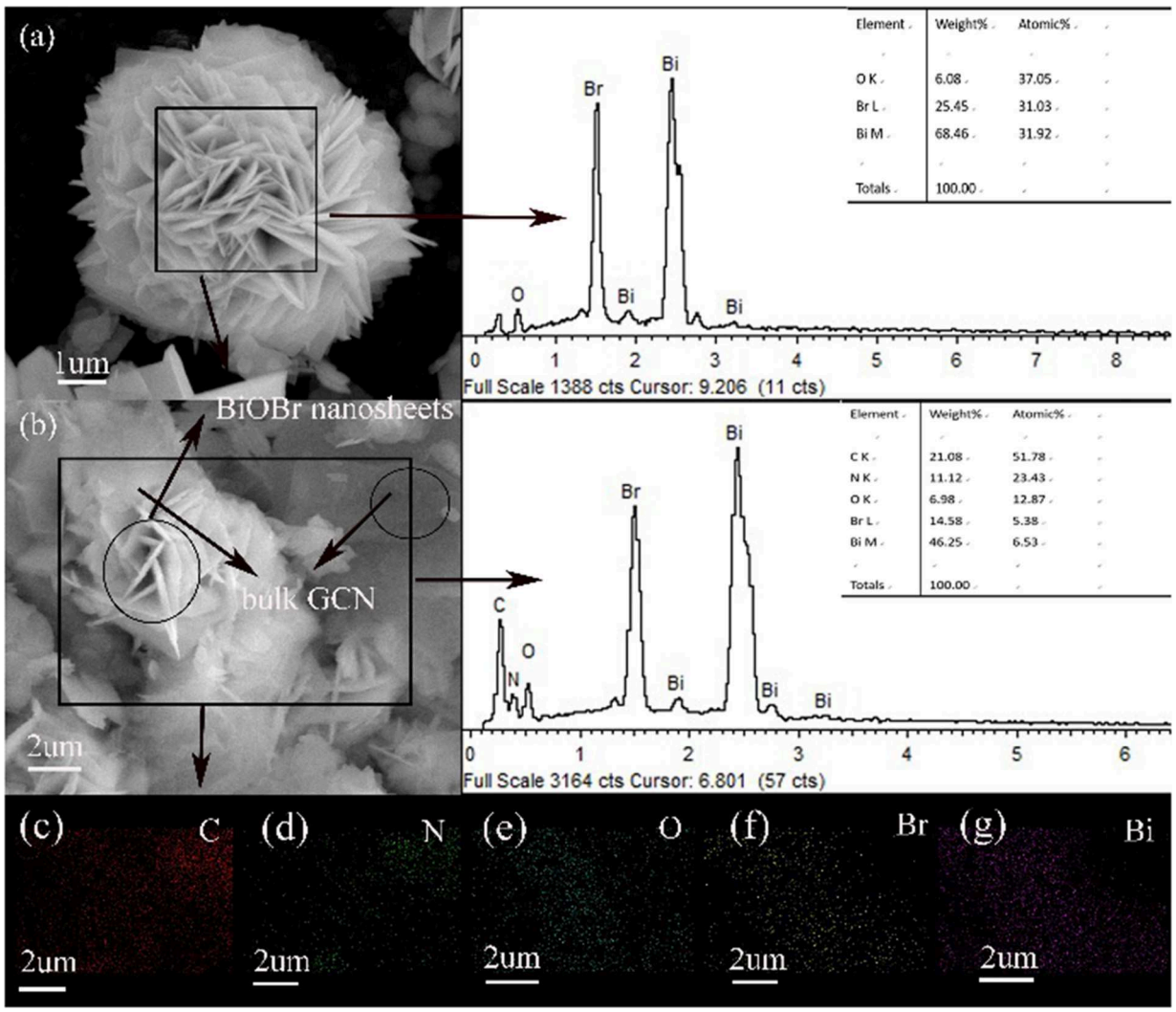

FIGURE 2 | SEM images of **(a)** pure BiOBr and **(b)** BiOBr-g-C_3N_4-4:1, elements mapping of BiOBr-g-C_3N_4-4:1.

of BiOBr and g-C_3N_4 at 464 nm and 437 nm were shown in **Figure 4**, which was consistent with the previous reports (Yan et al., 2009; Jiang et al., 2012b; Liao et al., 2012). The absorption edge of BiOBr-g-C_3N_4-4:1 is shifted to longer wavelength (at about 519 nm) than pure BiOBr and g-C_3N_4, due to the interaction between BiOBr and g-C_3N_4 (Wang et al., 2019). Moreover, the BiOBr-g-C_3N_4-4:1 photocatalyst possessed a strong absorption almost in the entire visible-light region. Herein, lots of electrons were excited to form free electrons and moved to the surface of catalyst. Furthermore, the band gap energies of photocatalysts were calculated by follow Kubelka-Munk formula (Luo et al., 2008; Cao et al., 2012):

$$\alpha h\nu = (h\nu - E_g)n \tag{1}$$

Where, α, ν, h, E_g means the absorption coefficient, light frequency, Planck's constant and band gap of semiconductors, respectively. In addition, the number (n) is depended on type of semiconductor ($n = 2$ for an indirect transition and $n = 1/2$ for a direct transition). For pure BiOBr and g-C_3N_4, the n is equal to 2. The band-gap energies of BiOBr, g-C_3N_4, and BiOBr-g-C_3N_4-4:1 photocatalysts were separately calculated to be 2.13, 2.47, and 1.80 eV, respectively. As a result, the low band gap is beneficial for the electrons transition from valence band to conduction band. The band edges of photocatalysts were estimated by using the following Equations (Chen et al., 2018):

$$E_{VB} = X - E_0 + 0.5E_g \tag{2}$$

$$E_{CB} = E_{VB} - E_g \tag{3}$$

The X stand for electronegativity of a semiconductor. The value for g-C_3N_4 and BiOBr are separately 4.72 and 6.45 eV, respectively. E_0 represents free electrons energy on the hydrogen scale (4.5 eV). Therefore, the valence band edge of BiOBr (+3.02 eV) is more positive than the valence band edge of g-C_3N_4

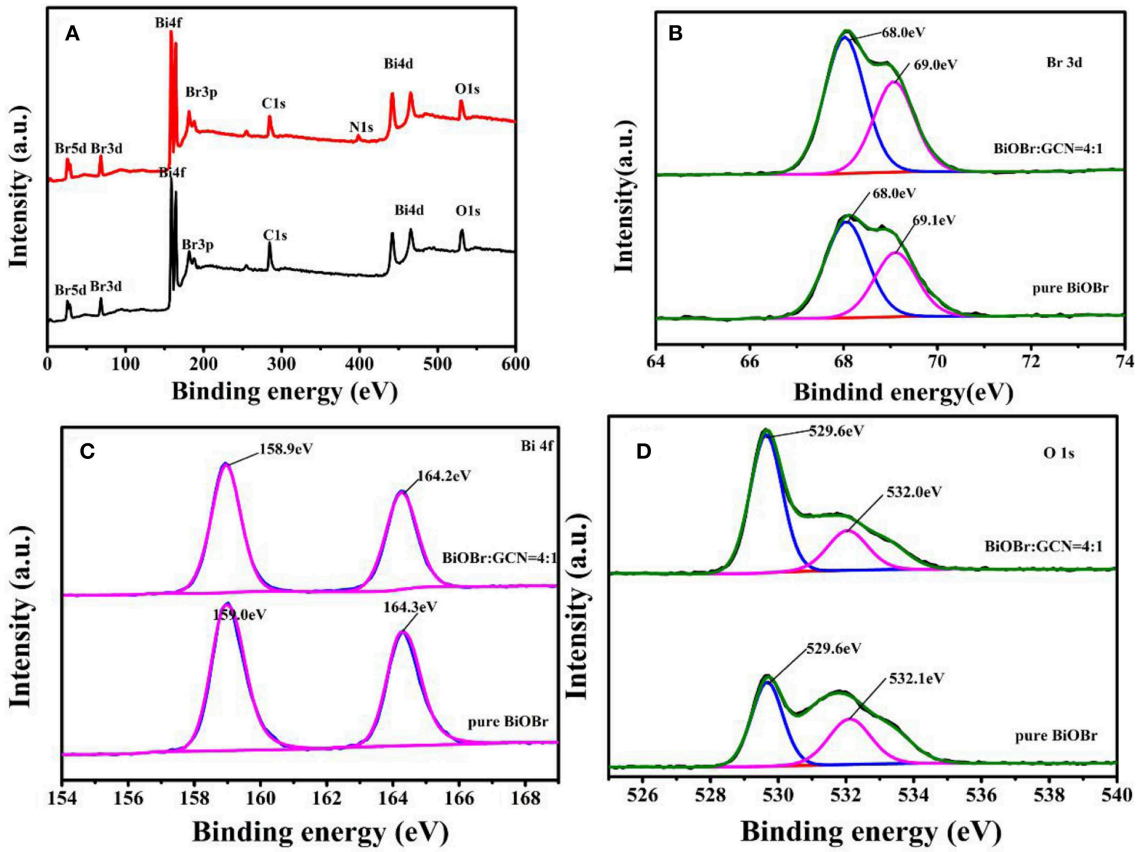

FIGURE 3 | XPS spectra of pure BiOBr and BiOBr-g-C_3N_4-4:1 composite; **(A)** survey, **(B)** Br 3d, **(C)** Bi 4f, and **(D)** O1s.

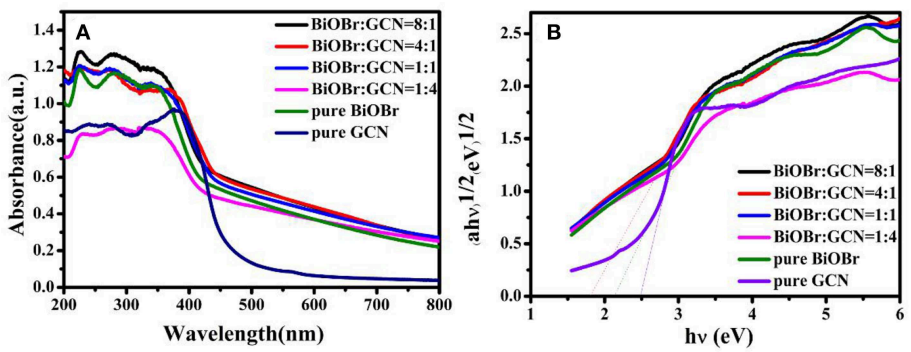

FIGURE 4 | (A) UV-vis diffuse reflectance spectra and **(B)** the band gap energies (E_g) of pure BiOBr and g-C_3N_4, BiOBr-g-C_3N_4 composites.

(+1.46 eV). Meantime, the conduction band edge of BiOBr (+0.89 eV) is more positive than the conduction band edge of g-C_3N_4 (−1.01eV). The electrons and holes were generated when electrons of valence band were excited under visible light irradiation and migrated from valence band to conduction band. Photogenerated holes on the VB of BiOBr were migrated to VB of g-C_3N_4 and photogenerated electrons on CB of g-C_3N_4 were migrated to CB of BiOBr. The formation of heterojunction promotes the separation of photogenerated electrons and holes and the redox reaction on the surface was efficient under visible-light irradiation (**Scheme 1**).

Photoluminescence (PL) spectra were utilized to analyze the separation efficiency and transportation of semiconductor photocatalysts. The electrons of the valence band were excited after light irradiation and transferred from VB to CB. However, rapid recombination occurred between electrons and holes due

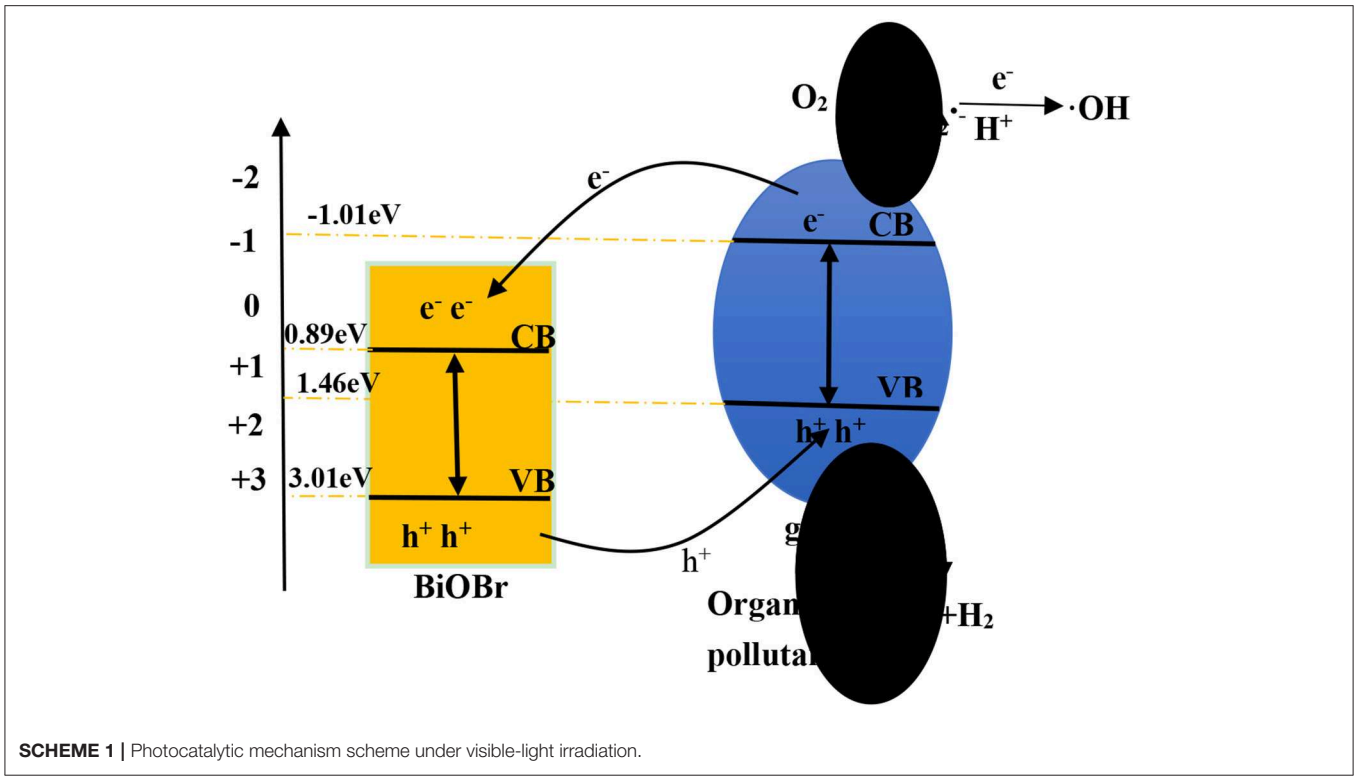

SCHEME 1 | Photocatalytic mechanism scheme under visible-light irradiation.

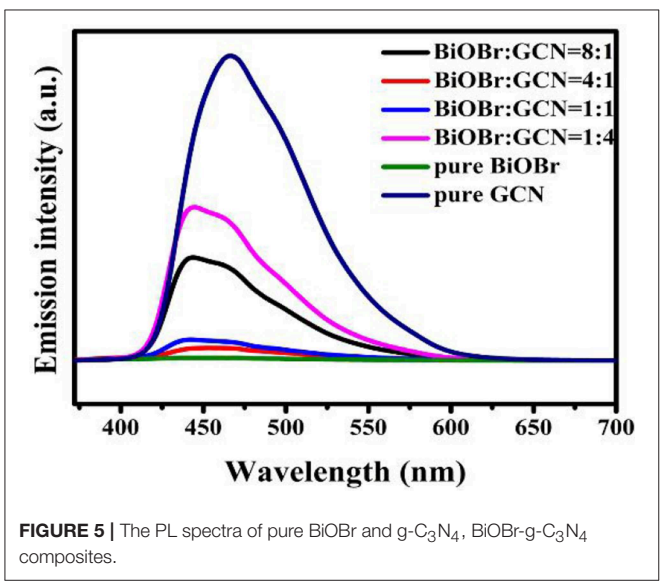

FIGURE 5 | The PL spectra of pure BiOBr and g-C_3N_4, BiOBr-g-C_3N_4 composites.

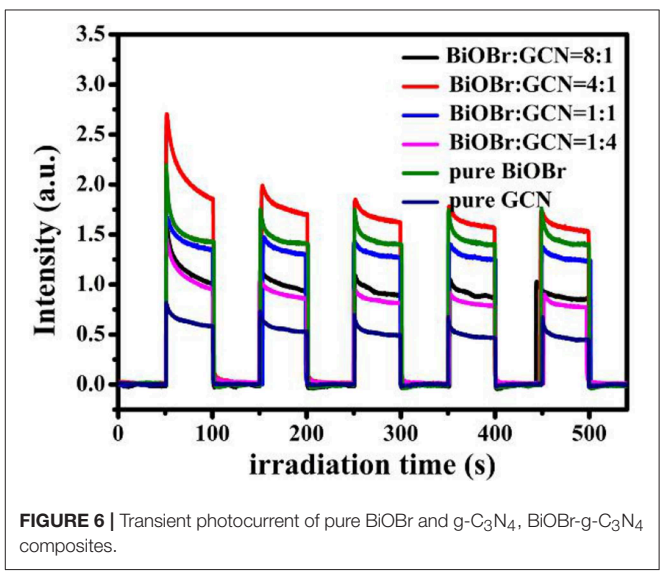

FIGURE 6 | Transient photocurrent of pure BiOBr and g-C_3N_4, BiOBr-g-C_3N_4 composites.

to the gravitational forces of between them, which is just like the force of gravity between man and earth. The PL emission peaks of BiOBr, g-C_3N_4, and composites were exhibited in **Figure 5**. The g-C_3N_4 exhibits a strongest emission peak at 466 nm. The blue shift occurred and the peak intensity decreased with the introduction of BiOBr to the heterojunction, and the BiOBr-g-C_3N_4-4:1 displayed the lowest emission peak intensity (**Figure 5**). Considering the fact that BiOBr-g-C_3N_4-8:1 even had a higher PL intensity than that of the BiOBr-g-C_3N_4-4:1, indicating that the low PL intensities of the BiOBr-g-C_3N_4 composites did not originate from the lower amounts of g-C_3N_4, but originated from the formation of the heterojunctions, which suppressed the recombination of the photo-generated charges. The band structure of two components in the composite matched well, which impeded the rapid recombination of photogenerated carries within the semiconductors. The lower emission peak intensity, the less possibility in the recombination of photogenerated carries. Moreover, there is not any observed

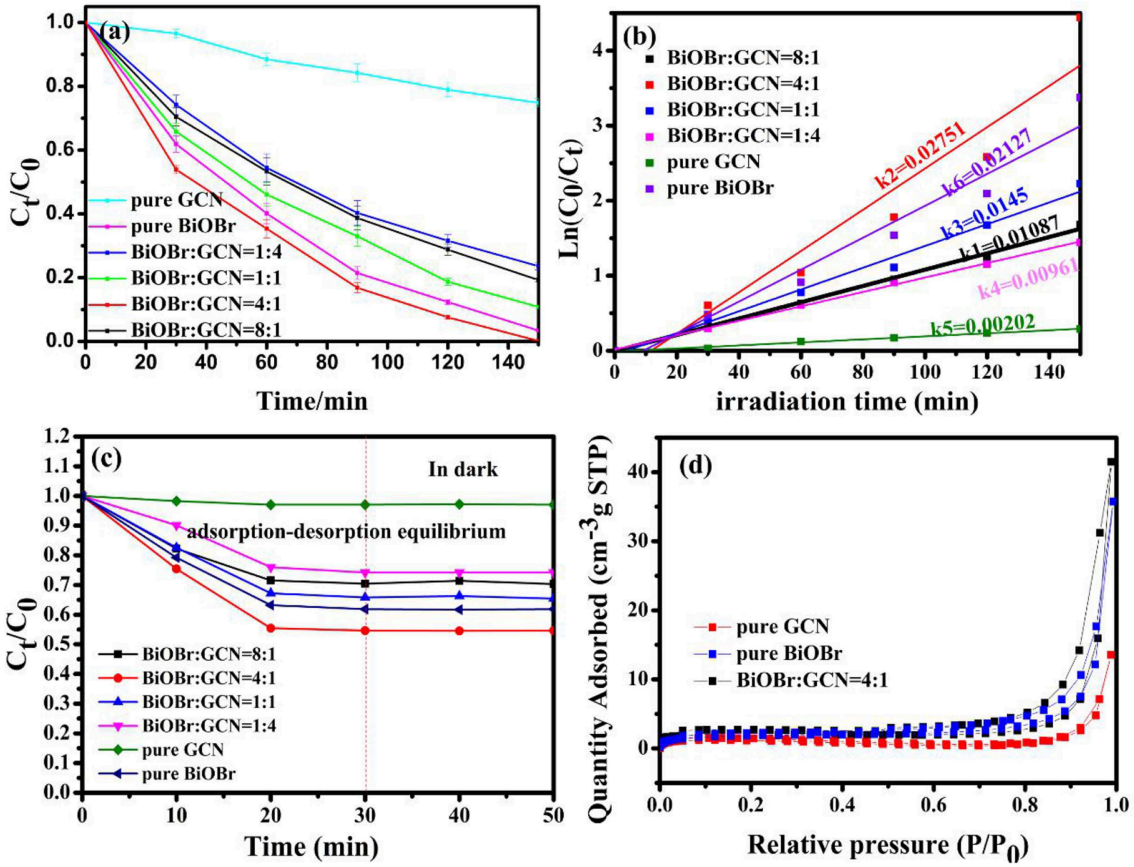

FIGURE 7 | (a) Photocatalytic activity; **(b)** plot of $\ln(C_0/C_t)$ vs. irradiation time over pure BiOBr and pure g-C_3N_4, BiOBr-g-C_3N_4 composites; **(c)** adsorption curves of BPA in the dark; **(d)** N_2 adsorption-desorption isotherms curves.

PL signal for the pure BiOBr, indicating that no radiative recombination of photo-generated charges occurred for the pure BiOBr (Sun et al., 2014; Huang et al., 2015a). In summary, the BiOBr-g-C_3N_4 heterojunctions were synthesized successfully, and BiOBr provides little electrons separately. The electrons mainly originated from g-C_3N_4 and flow from the g-C_3N_4 to the surface of BiOBr. The tight contact between BiOBr and g-C_3N_4 offers a convenient access, which increases the transfer rate of photogenerated electrons.

For offering further evidence to support the enhanced separation efficiency of photogenerated carries, the transient photocurrent-time curves of pure BiOBr and g-C_3N_4 were shown in **Figure 6**, together with BiOBr-g-C_3N_4 composites. The higher the photocurrent intensity, the better the photocatalytic activity is. It is the common understanding on the relationship between photocurrent and photocatalytic activity. As shown in **Figure 6**, the current reached rapidly to the stable state when on the light irradiation was turned on and decreased suddenly after the light turning off. The photocurrent can be maintained to a large extent of the original value after five cycles of the exposure to the on-off switchable irradiation.

BiOBr-g-C_3N_4-4:1 exhibited the highest intensity of photocurrent among the samples, indicating that the heterostructure in BiOBr-g-C_3N_4 composite greatly inhibited the recombination of photogenerated carries and extends the lifetime of photoinduced electrons (Huang et al., 2015b, 2016).

TABLE 1 | The parameters obtained from the nitrogen adsorption/desorption of composite.

Sample	BET surface/m^2g^{-1}	Pore volume/cm	Band gap/eV
Pure BiOBr	5.9906	0.0551	2.13
Pure GCN	2.8643	0.0209	2.47
BiOBr/g-C_3N_4-4:1	6.0396	0.0642	1.80

Photocatalytic Studies

The photocatalytic degradation of BPA was utilized to test the degradation efficiency of samples with the cutting off of ultraviolet light ($\lambda < 420$ nm). In order to reaching adsorption-desorption equilibrium, the catalyst/BPA solution mixture was stirred for 30 min in the dark. The photocatalytic efficient and error bar were shown in **Figure 7a**, the BiOBr-g-C_3N_4-4:1 material exhibited higher photocatalytic performance than other catalysts prepared previously. The BPA was completely removed

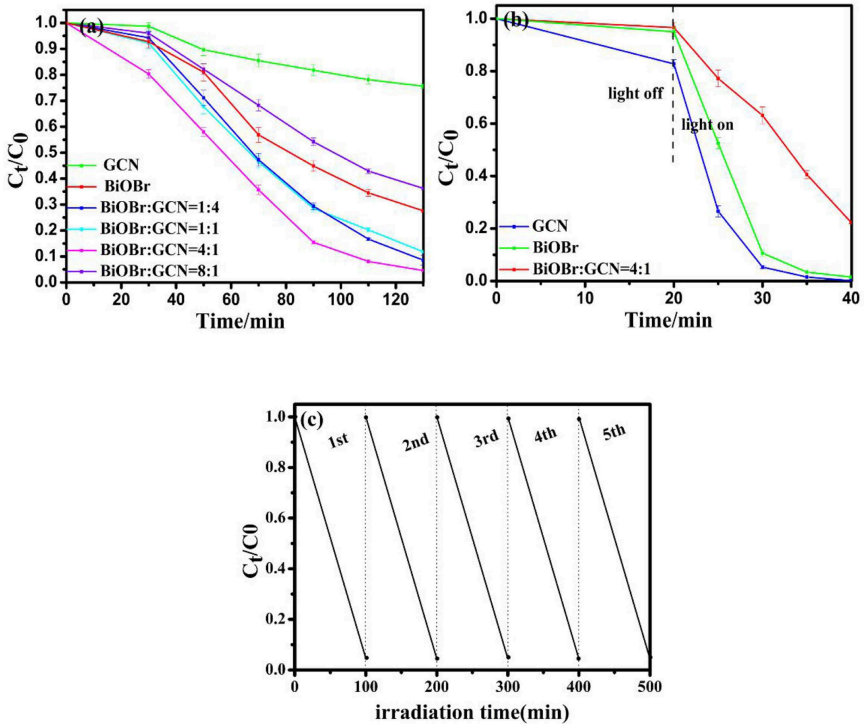

FIGURE 8 | Degradation of **(a)** MO and **(b)** RhB over pure BiOBr, g-C_3N_4 and BiOBr-g-C_3N_4 composites; **(c)** Recycling tests of BiOBr-g-C_3N_4-4:1 photocatalyst on the degradation of MO.

within 120 min under visible-light irradiation for the composite catalyst. However, for pure BiOBr and g-C_3N_4, 96.6 and 25.2% of BPA were removed, respectively, during the same incubation time. To further investigate the adsorption performance in the dark condition, the catalysts was added into BPA solution as the light was turned off. As was shown in **Figure 7c**, it can be found that BiOBr/g-C_3N_4-4:1 showed the best adsorption capacity, and it showed that almost 50% of BPA was adsorbed in 30 min. The phenomenon was consistent with result of N_2 adsorption-desorption isotherms curves in **Figure 7d**. The BET surface area and pore volume of samples were measured, and the result was shown in **Figure 7d** and **Table 1**. For three catalysts, the isotherms curves exhibited a type IV curve and type H3 hysteresis loops at the relative pressure of 0.5–1.0. The following pseudo-first-order kinetics equation was used to compare the degradation efficiencies of samples (Fu et al., 2018; Zeng et al., 2018):

$$\mathrm{In}(C_0/C_t) = k^*t \quad (4)$$

Where, C_0 and C_t are the BPA concentrations in solution at time of 0 and t, respectively. The k represents the first-order kinetics rate constant. The result was shown in **Figure 7b**, which was consistent with above analysis. The BiOBr-g-C_3N_4-4:1 exhibited the maximum rate constant of 0.02751 min^{-1}, being 1.29 and 13.6 times of pure BiOBr and g-C_3N_4 photocatalysts, respectively.

Photocatalytic degradation of methyl orange (MO) and rhodamine B (RhB) over BiOBr, g-C_3N_4, and BiOBr-g-C_3N_4 composites were applied to further analyze photocatalytic efficiencies of degrading organic pollutants under visible-light irradiation. As shown in **Figure 8**, the BiOBr-g-C_3N_4-4:1 still possessed the highest photocatalytic activity among all samples prepared. 95.5% of MO was decolored in 100 min and 99.9% of RhB was decolored in 20 min over BiOBr-g-C_3N_4-4:1 composite. The result demonstrated that BiOBr-g-C_3N_4 possessed the ability of degrading organic pollutants in wastewater under visible-light irradiation, with BiOBr-g-C_3N_4-4:1 possessed the highest photocatalytic activity. The stability of BiOBr-g-C_3N_4-4:1 photocatalyst was further investigated by repeated degradation of MO under visible-light irradiation. The photocatalytic activity showed a slight decrease after five cycles. It was proved that BiOBr-g-C_3N_4-4:1 exhibited excellent stability.

Photocatalytic Mechanism

As we all know, active species, such as $O_2^{\bullet-}$, h^+, and •OH radical, according to previous reports, play an important role during the photocatalytic degradation process (Fu et al., 2005; Yang et al., 2015; Huang et al., 2017c). Herein, the active species trap experiment over the BiOBr-g-C_3N_4 photocatalyst was carried out with the illumination of visible light. The results of photocatalytic degradation with addition of ethylenediaminetetraacetate (EDTA, a quencher of h^+), benzoquinone(BQ, a quencher of $O_2^{\bullet-}$), and tert-butyl alcohol(TBA, a quencher of •OH) were

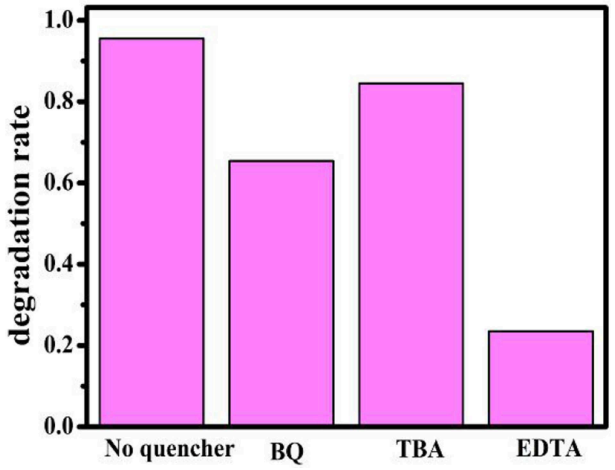

FIGURE 9 | Trapping experiment of active species under visible-light irradiation.

shown in **Figure 9**. Degradation of MO was used to achieve this process. For comparison, the experiment was carried out without addition of any scavenger. It was obviously found that photocatalytic efficiency of MO decrease when EDTA and BQ were added into the solution. It turns out that h^+ and $O_2^{\bullet-}$ was the main active radical in the photocatalytic reaction of MO.

According to the above calculated band-gap edge, a possible photocatalytic mechanism was proposed to explain the process of photocatalytic degradation reaction. The conduction band (CB) potential of g-C_3N_4 (−1.01 eV vs. NHE) is negative than the standard redox potential of $O_2/O_2^{\bullet-}$(−0.046 eV vs. NHE) (Cui et al., 2012). So, free radical $O_2^{\bullet-}$ were produced from adsorbed oxygen molecule due to reduction of the electrons in the CB of g-C_3N_4. However, the standard redox potential of Bi^{4+}/Bi^{3+} (1.59 eV) is negative than E_0 ($\bullet OH/OH^- = +1.99$ eV vs. NHE) (Fu et al., 2005). It can be concluded that •OH could not be obtained on the VB of BiOBr and g-C_3N_4. Actually, O_2 dissolved into water might be reduced to •OH by a two-electron oxidation pathway (Fu et al., 2005; Kanagaraj and Thiripuranthagan, 2017). As a result, the BiOBr-g-C_3N_4-4:1 exhibited higher photocatalytic performance than pure BiOBr and g-C_3N_4. Meantime, the band gap of BiOBr-g-C_3N_4-4:1 is lower than pure photocatalysts. It can be deduced that electrons in the CB of g-C_3N_4 were transferred to the CB of BiOBr, which was consistent with PL result.

CONCLUSION

In summary, we have reported a simple hydrothermal method to synthesize successfully flower-like BiOBr and BiOBr-g-C_3N_4 composites. The results displayed that g-C_3N_4 were deposited on the surface of BiOBr nanosheets to form a tight contactheterostructure between BiOBr and g-C_3N_4 nanoflakes. The band gap of BiOBr-g-C_3N_4 heterojunction was narrower than the band gap of pure BiOBr nanosheet bulk g-C_3N_4, which was propitious to the transfer of photogenerated electrons from valence band to conduction band. Moreover, the BiOBr-g-C_3N_4-4:1 exhibited the highest photocatalytic performance for the degradation of BPA under visible light irradiation due to its superior quantum efficiency. The PL results demonstrated that the charges were offered mainly by g-C_3N_4 and moved from CB of g-C_3N_4 to CB of BiOBr. The band edges of the composites were shifted to longer wavelength than pure BiOBr with the loading of g-C_3N_4. In order to evaluate the degradation performance of organic pollutants in wastewater, degradation of MO and RhB under visible light irradiation were also carried out at room temperature. The result demonstrated that the composite photocatalyst possessed excellent photocatalytic performance in the degradation of organic pollutants. Last but not least, a possible mechanism was proposed in photocatalytic reaction.

DATA AVAILABILITY STATEMENT

The datasets generated for this study are available on request to the corresponding author.

AUTHOR CONTRIBUTIONS

JW performed experiments and drafted the manuscript. YX provided the idea and guided the undertaken of the experiments. YL helped to discuss some of the experimental results. YD took the instrumental analysis and analyzed the data. JL and SL discussed the mechanisms of the photocatalysis reaction. JZ polished the language of the manuscript.

FUNDING

This work was financially supported by the National Natural Science Foundation of China (No. 21667019), the Key Project of Natural Science Foundation of Jiangxi Province (No. 20171ACB20016), the Jiangxi Province Major Academic and Technical Leaders Cultivating Object Program (No. 20172BCB22014), the Science and Technology Department of Jiangxi Province (No. 20181BCB18003 and 20181ACG70025), the Key Laboratory of Photochemical Conversion and Optoelectronic Materials, TIPC, CSA (No. PCOM201906), and the Key Project of Science and Technology Research of the Jiangxi Provincial Department of Education (No. DA201602063), and Fujian Key Laboratory of Measurement and Control System for of Shore Environment (No. S1-KF1703).

REFERENCES

Cao, J., Luo, B. D., Lin, H. L., Xu, B. Y., and Chen, S. F. (2012). Thermo decomposition synthesis of WO_3/H_2WO_4 heterostructures with enhanced visible light photocatalytic properties. *Appl. Cataly. B-Environ.* 111, 288–296. doi: 10.1016/j.apcatb.2011.10.010

Chang, F., Xie, Y. C., Li, C. L., Chen, J., Luo, J. R., Hu, X. F., et al. (2013). A facile modification of g-$C_3N_4$with enhanced photocatalytic

activity for degradation of methylene blue. *Appl. Surf. Sci.* 280, 967–974. doi: 10.1016/j.apsusc.2013.05.127

Chen, D. D., Wu, S. X., Fang, J. Z., Lu, S. Y., Zhou, G. Y., Feng, W. H., et al. (2018). A nanosheet-like α-Bi_2O_3/g-C_3N_4 heterostructure modified by plasmonic metallic Bi and oxygen vacancies with high photodegradation activity of organic pollutant. *Sep. Purif. Technol.* 193, 232–241. doi: 10.1016/j.seppur.2017.11.011

Chen, D. M., Wang, K. W., Xiang, D. G., Zong, R. L., Yao, W. Q., and Zhu, Y. F. (2014). Significantly enhancement of photocatalytic performances via core-shell structure of ZnO@mpg-C_3N_4. *Appl. Catal. B-Environ.* 147, 554–561. doi: 10.1016/j.apcatb.2013.09.039

Chen, F., Huang, H., Guo, L.,Zhang, Y., and Ma, T. (2019). The role of polarization in photocatalysis. *Angew. Chem. Int. Ed.* 58, 10061–10073, doi: 10.1002/anie.201901361

Cheng, H. F., Huang, B. B., Wang, P., Wang, Z. Y., Lou, Z. Z., Wang, J. P., et al. (2011). In situ ion exchange synthesis of the novel Ag/AgBr/BiOBr hybrid with highly efficient decontamination of pollutants. *Chem. Commun.* 47, 7054–7056. doi: 10.1039/c1cc11525a

Chi, S. H., Ji, C. N., Sun, S. W., Jiang, H., Qu, R. J., and Sun, C. M. (2016). Magnetically separated maso-g-C3N4/Fe3O4: bifunctional composites for removal of arsenite by simultaneous visible-light catalysis and adsorption. *Ind. Eng. Chem. Res.* 55, 12060–12067. doi: 10.1021/acs.jecr.6b02178

Cui, Y. J., Huang, J. H., Fu, X. Z., and Wang, X. C. (2012). Metal-free photocatalytic degradation of 4-chlorophenol in water by mesoporous carbon nitride semiconductor. *Catal. Sci. Technol.* 2, 1396–1402. doi: 10.1039/c2cy20036h

Di, J., Xia, J. X., Ji, M. X., Wang, B., Yin, S., Zhang, Q., et al. (2015). Carbon quantum dots modified BiOCl ultrathin nanosheets with enhanced molecular oxygen activation ability for broad spectrum photocatalytic properties and mechanism insight. *ACS. Appl. Mater. Inter.* 7:20111. doi: 10.1021/acsami.5b05268

Fu, H. B., Pan, C. S., Yao, W. Q., and Zhu, Y. F. (2005). Visible-light-induced degradation of rhodamine B by nanosized Bi_2WO_6. *J. Phys. Chem. B.*109:22432. doi: 10.1021/jp052995j

Fu, H. H., Yang, L. M., Hua, D. S., Yu, C., Ling, Y., Xie, Y., et al. (2018). Titanium dioxide nano-heterostructure with nanoparticles decorating nanowires for high-performance photocatalysis. *Int. J. Hydrogen. Energy*. 43, 10359–10367. doi: 10.1016/j.ijhydene.2018.04.150

Fu, J., Tian, Y. L., Chang,B. B., Xi, F. N., and Dong, X.P. (2012). BiOBr-carbon nitride heterojunctions: synthesis, enhanced activity and photocatalytic mechanism. *J. Mater. Chem*. 22, 21159–21166. doi: 10.1039/c2jm34778d

Fujishima, A., and Honda, K. (1972). Electrochemical photolysis of water at a semiconductor electrode. *Nature*. 238, 37–38. doi: 10.1038/238037a0

Goettmann, F., Fischer, A., Antonietti, M., and Thomas, A. (2006). Chemical synthesis of mesoporous carbon nitrides using hard templates and their use as a metal-free catalyst for Friedel-crafts reaction of benzene. *Angew. Chem. Int. Ed*. 45, 4467–4471. doi: 10.1002/anie.200600412

Groenewolt, M., and Antonietti, M. (2005). Synthesis of g-C_3N_4 nanoparticles in mesoporous silica host matrices. *Adv. Mater.* 17, 1789–1792. doi: 10.1002/adma.200401756

Hao, L., Kang, L., Huang, H., Ye, L., Han, K., Yang, S., et al. (2019). Surface-halogenation-induced atomic-site activation and local charge separation for superb CO_2 photoreduction. *Adv. Mater.* 31:1900546. doi: 10.1002/adma.201900546

Huang, H., Cao, R., Yu, S., Xu, K., Hao, W., Wang, Y., et al. (2017a). Single-unit-cell layer established Bi_2WO_6 3D hierarchical architectures: efficient adsorption, photocatalysis and dye-sensitized photoelectrochemical performance. *Appl. Catal. B: Environ*. 219, 526–537. doi: 10.1016/j.apcatb.2017.07.084

Huang, H., Han, X., Li, X., Wang, S., Chu, P., and Zhang, Y. (2015a). Fabrication of multiple heterojunctions with tunable visible-light-active photocatalytic reactivity in BiOBr-BiOI full-range composites based on microstructure modulation and band structures. *ACS Appl. Mater. Interf.* 7, 482–492. doi: 10.1021/am5065409

Huang, H., Li, X., Wang, J., Dong, F., Chu, P., Zhang, T., et al. (2015b). Anionic group self-doping as a promising strategy: band-gap engineering and multi-functional applications of high-performance CO_3^{2-}-doped $Bi_2O_2CO_3$. *ACS Catalysis*. 5, 4094–4103. doi: 10.1021/acscatal.5b00444

Huang, H., Tu, S., Zeng, C., Zhang, T., Reshak, A., and Zhang, Y. (2017c). Macroscopic polarization enhancement promoting photo- and piezoelectric-induced charge separation and molecular oxygen activation. *Angew. Chem. Int. Ed*. 56, 11860–11864. doi: 10.1002/anie.201706549

Huang, H., Xiao, K., He, Y., Zhang, T., Dong, F., Du, X., et al. (2016). *In situ* assembly of BiOI@$Bi_{12}O_{17}Cl_2$ p-n junction: charge induced unique front-lateral surfaces coupling heterostructure with high exposure of BiOI {001} active facets for robust and nonselective photocatalysis. *Appl. Catal. B: Environ*. 199, 75–86. doi: 10.1016/j.apcatb.2016.06.020

Huang, H., Xiao, K., Zhang, T., Dong, F., and Zhang, Y. (2017b). Rational design on 3D hierarchical bismuth oxyiodides via in situ self-template phase transformation and phase-junction construction for optimizing photocatalysis against diverse contaminants. *Appl. Catal. B: Environ*. 203, 879–888. doi: 10.1016/j.apcatb.2016.10.082

Huang, W. L., and Zhu, Q. (2008). Electronic structure of relaxed BiOX (X=F, Cl, Br, I) photocatalysts. *Comput. Mater. Sci*. 43, 1101–1108. doi: 10.1016/j.commatsci.2008.03.005

Huo, Y. N., Zhang, J., Miao, M., and Jin, Y. (2012). Solvothermal synthesis of flower-like BiOBr microspheres with highly visible-light photocatalytic performances. *Appl. Catal. B-Environ.* 111, 334–341. doi: 10.1016/j.apcatb.2011.10.016

Jiang, J., Zhao, K., Xiao, X., and Zhang, L. (2012a). Synthesis and facet-dependent photoreactivity of BiOCl single-crystalline nanosheets. *J. Am. Chem. Soc*. 134, 4473–4476. doi: 10.1021/ja210484t

Jiang, Z., Yang, F., Yang, G. D., Kong, L., Jones, M. O., Xiao, T. C., et al. (2012b). The hydrothermal synthesis of BiOBr flakes for visible-light-responsive photocatalytic degradation of methyl orange. *J. Photochem. Photobiol. A.* 212, 8–13. doi: 10.1016/j.jphotochem.2010.03.004

Kanagaraj, T., and Thiripuranthagan, S. (2017). Photocatalytic activities of novel SrTiO3-BiOBr heterojunction catalysts towards the degradation of reactive dyes. *Appl. Catal. B Environ*. 207, 218–232. doi: 10.1016/j.apcatb.2017.01.084

Kijima, N., Matano, K., Saito, M., Oikawa, T., Konishi, T., Yasuda, H., et al. (2001). Oxidative catalytic cracking of n-butane to lower alkenes over layered BiOCl catalyst. *Appl. Catal. A-Gen.* 206, 237–244. doi: 10.1016/S0926-860X(00)00598-6

Kong, L., Jiang, Z., Lai, H. H., Nicholls, R. J., Xiao, T. C., Jone, M. O., et al. (2012).Unusual reactivity of visible-light-responsive AgBr-BiOBr heterojunction photocatalysts. *J. Catal.* 293, 116–125. doi: 10.1016/j.jcat.2012.06.011

Kuang, P. Y., Su, Y. Z., Chen, G. F., Luo, Z., Xing, S. Y., Li, N., et al. (2015). g-C_3N_4 decorated ZnO nanorod arrays for enhanced photoelectrocatalytic performance. *Appl. Surf. Sci.* 358, 296–303. doi: 10.1016/j.apsusc.2015.08.066

Kusainova, A. M., Lightfoot, P., Zhou, W. Z., Stefanovich, S. Y., Mosunov, A. V., and Dolgikh, V. A. (2001). Ferroelectric properties and crystal structure of the layered intergrowth phase $Bi_3Pb_2Nb_2O_{11}$. *Chem. Mater.* 13, 4731–4737. doi: 10.1021/cm011145n

Lei, Y. Q., Wang, G. H., Song, S. Y., Fan, W. Q., Pang, M., Tang, J. K., et al. (2010). Room temperature, template-free synthesis of BiOI hierarchical structure: visible-light photocatalytic and electrochemical hydrogen storage properties. *Dalton T.* 3273–3278. doi: 10.1039/b922126c

Li, Q., Zhang, N., Yang, Y., Wang, G. Z., and Ng, D. H. L. (2014). High efficiency photocatalysis for pollutant degradation with MoS_2/C_3N_4 heterostructures. *Langmuir* 30, 8965–8972. doi: 10.1021/la502033t

Liang, F. F., and Zhu, Y. F. (2016). Enhancement of mineralization ability for phenol via synergetic effect of photoelectrocatalysis of g-C_3N_4 film. *Appl. Catal. B:-Environ.* 180, 324–329. doi: 10.1016/j.apcatb.2015.05.009

Liao, G. Z., Chen, S., Quan, X., Yu, H. T., and Zhao, H. M. (2012). Graphene oxide modified g-C_3N_4 hybrid with enhanced photocatalytic capability under visible light irradiation. *J. Mater. Chem*. 22, 2721–2726. doi: 10.1039/C1JM13490F

Liu, G., Niu, P., Sun, C. H., Smith, S. C., Chen, Z. G., Lu, G. Q., et al. (2010). Unique electronic structure induced high photoreactivity of sulfur-doped graphitic C_3N_4. *J. Am. Chem. Soc*. 132, 11642–11648. doi: 10.1021/ja103798k

Liu, H.,Su, Y., Chen, Z., Jin, Z. T., and Wang, Y. (2014). Graphene sheets grafted three-dimensional $BiOBr_{0.2}I_{0.8}$ microspheres with excellent photocatalytic activity under visible light. *J. Hazard. Mater.* 266, 75–83. doi: 10.1016/j.jhazmat.2013.12.013

Liu, Y. Y., Xie, Y.u, Ling, Y., Jiao, J. L., Li, X., and Zhao, J. S. (2019). Facile construction of a molybdenum disulphide/zinc oxide nanosheet hybrid for an advanced photocatalyst. *J. Alloy. Compd*. 778, 761–767. doi: 10.1016/j.jallcom.2018.11.024

Lu, X. L., Xu, K., Chen, P. Z., Jia, K. C., Liu, S., and Wu, C. Z. (2014). Facile one step method realizing scalable production of g-C_3N_4 nanosheets and study of their photocatalytic H_2 evolution activity. *J. Mater. Chem A*. 2, 18924–18928. doi: 10.1039/C4TA04487H

Luo, W. J., Tang, J. W., Zou, Z. G., and Ye, J. H. (2008). Preparation and photophysical properties of some oxides in Ca-Bi-O system. *J. Alloys. Compd.* 455, 346–352. doi: 10.1016/j.jallcom.2007.01.096

Maeda, K.,Teramura, K., Lu, D. L., Takata, T., Saito, N., Inoue, Y., and Domen, K. (2006). Photocatalyst releasing hydrogen from water. *Nature* 440, 295–295. doi: 10.1038/440295a

Maile, F., Pfaff, G., and Reynders, P. (2005). Effect pigments-past, present and future. *Prog. Org. Coat.* 54, 150–163. doi: 10.1016/j.porgcoat.2005.07.003

Osterloh, F. E. (2008). Inorganic materials as catalysts for photochemical splitting of water. *Chem. Mater.* 39, 35–54. doi: 10.1021/cm7024203

Peng, B. Y., Zhang, S. S., Yang, S. Y., Wang, H. J., Yu, H., Zhang, S. Q., et al. (2014). Synthesis and characterization of g-C_3N_4/Cu_2O composite catalyst with enhanced photocatalytic activity under visible light irradiation. *Mater. Res. Bull.* 56, 19–24. doi: 10.1016/j.materresbull.2014.04.042

Santato, C., Ulmann, M., and Augustynski, J. (2001). Enhanced visible light conversion efficiency using nanocrystalline WO_3 films. *Adv. Mater.* 13, 511–514. doi: 10.1002/1521-4095(200104)13:7<511::AID-ADMA511>3.0.CO;2-W

Shang, M., Wang, W., and Zhang, L. (2009). Preparation of BiOBr lamellar structure with high photocatalytic activity by CTAB as Br source and template. *J. Hazard. Mater.* 167, 803–809. doi: 10.1016/j.jhazmat.2009.01.053

Stasinakis, A. S.,Petalas, A. V., Mamais,D., and Thomaidis, N.S. (2008). Application of the OECD 301F respirometric test for the biodegradability assessment of various potential endocrine disrupting chemicals. *Bioresour. Technol.* 99, 3458–3467. doi: 10.1016/j.biortech.2007.08.002

Sun, C. Y., Xu, Q. H., Xie, Y., Ling, Y., Jiao, J. L., Zhu, H. H., et al. (2017). High-efficient one-pot synthesis of carbon quantum dots decorating Bi_2MoO_6 nanosheets heterostructure with enhanced visible-light photocatalytic properties. *J. Alloy. Compd*, 723, 333–344. doi: 10.1016/j.jallcom.2017.06.130

Sun, Y. J., Zhang, W. D., Xiong, T., Zhao, Z. W., Dong, F., Wang, R. Q., et al. (2014). Growth of BiOBr nanosheets on C_3N_4 nanosheets to construct two-dimensional nanojunctions with enhanced photoreactivity for NO removal. *J. Colloid. Interface. Sci.* 418, 317–323. doi: 10.1016/j.jcis.2013.12.037

Tsai, W. (2006). Human health risk on environmental exposure to bisphenol-A: a review. *J. Environ. Health. Sci.* 24, 225–255. doi: 10.1080/10590500600936482

Vinu, A., Ariga, K., Mori, T., Nakanishi, T., Hishita, S., Golberg, D., et al. (2005). Preparation and characterization of well-ordered hexagonal mesoporous carbon nitride. *Adv. Mater.* 17, 1648–1652. doi: 10.1002/adma.200401643

Wang, J. J., Tang, L., Zeng, G. M., Deng, Y. C., Liu, Y. N., Wang, L. L., et al. (2017).Atomic scale g-C_3N_4/Bi_2WO_6 2D/2D heterojunction with enhanced photocatalytic degradation of ibuprofen under visible light irradiation. *Appl. Catal. B-Environ.* 209, 285–294. doi: 10.1016/j.apcatb.2017.03.019

Wang, X. C., Chen, X. F., Thomas, A., Fu, X. Z., and Antonietti, M. (2010). Metal-containing carbon nitride compounds: a new functional organic-metal hybrid material. *Adv. Mater.* 21, 1609–1612. doi: 10.1002/adma.200802627

Wang, X. J., Yang, W. Y., Li, F. T., Zhao, J., Liu, R. H., Liu, S. J., et al. (2015). Construction of amorphous TiO_2/BiOBr heterojunctions via facets coupling for enhanced photocatalytic activity. *J. Hazard. Mater.* 292, 126–136. doi: 10.1016/j.jhazmat.2015.03.030

Wang, Y.;, Wang, X. C., and Antonietti, M. (2012). Polymeric graphitic carbon nitride as a heterogeneous organocatalyst: from photochemistry to multipurpose catalysis to sustainable chemistry. *Angew. Chem. Int. Ed.* 51, 68–89. doi: 10.1002/anie.201101182

Wang, Z. Z., Wang, K., Li, Y., Jiang, L. S., and Zhang, G. K. (2019). Novel BiSbO4/BiOBr nanoarchitecture with enhanced visible-light driven photocatalytic performance: oxygen-induced pathway of activation and mechanism unveiling. *Appl. Surf. Sci*. doi: 10.1016/j.apsusc.2019.143850. [Epub ahead of print].

Wu, W., Shan, G. Q., Wang, S. F., Zhu, L., Y., Yue, L. F., et al. (2016). Environmentally relevant impacts of nano-TiO_2 on abiotic degradation of bisphenol A under sunlight irradiation. *Environ. Pollut.* 216, 166–172. doi: 10.1016/j.envpol.2016.05.079

Yan, H. J. (2012). Soft-templating synthesis of mesoporous graphitic carbon nitride with enhanced photocatalytic H_2 evolution under visible light. *Chem. Commun.* 48, 3430–3432. doi: 10.1039/c2cc00001f

Yan, S. C., Li, Z. S., and Zou, Z. G. (2009). Photodegradation performance of g-C_3N_4 fabricated by directly heating melamine. *Langmuir* 25, 10397–10401. doi: 10.1021/la900923z

Yan, S. C., Li, Z. S., and Zou, Z. G. (2010). Photodegradation of rhodamine B and methyl orange over boron-doped g-C_3N_4 under visible light irradiation. *Langmuir* 26, 3894–3901. doi: 10.1021/la904023j

Yang, Q., Zhong, J. B., Li, J. Z., Chen, J. F., Xiang, Z., Wang, T., et al. (2017). Photo-induced charge separation properties of NiO/Bi_2O_3 heterojunctions with efficient simulated solar-driven photocatalytic performance. *Curr. Appl. Phys.* 17, 484–487. doi: 10.1016/j.cap.2017.01.019

Yang, Z. C., Li, J., Cheng, F. X., Chen, Z., and Dong, X. P. (2015). BiOBr/protonated graphitic C_3N_4 heterojunctions: intimate interfaces by electrostatic interaction and enhanced photocatalytic activity. *J. Alloys Compd*. 634, 215–222. doi: 10.1016/j.jallcom.2015.02.103

Ye, L. Q., Liu, J. Y., Jiang, Z., Peng, T. Y., and Zan, L. (2013). Facets coupling of BiOBr-g-C_3N_4 composite photocatalyst for enhanced visible-light-driven photocatalytic activity. *Appl. Catal. B-Environ*. 142–143, 1–7. doi: 10.1016/j.apcatb.2013.04.058

Ye, L. Q., Zan, L., Tian, L.,H; Peng, T. Y., and Zhang, J. J. (2011). The {001} facets-dependent high photoactivity of BiOCl nanosheets. *Chem. Commun.* 47, 6951–6953. doi: 10.1039/c1cc11015b

Zeng, D. D., Yang, L. M., Zhou, P. P., Hua, D. S., Xie, Y., Li, S. Q., et al. (2018). AuCu alloys deposited on titanium dioxide nanosheets for efficient photocatalytic hydrogen evolution. *Int. J. Hydrogen. Energy* 43, 15155–15163. doi: 10.1016/j.ijhydene.2018.06.078

Zhang, K. L., Liu, C. M., Huang, F. Q., Zheng, C., and Wang, W. D. (2006). Study of the electronic structure and photocatalytic activity of the BiOCl photocatalyst. *Appl. Catal. B-Environ.* 68, 125–129. doi: 10.1016/j.apcatb.2006.08.002

Zhang, S. J., Chen, X. X., and Song, L. M. (2019). Preparation of BiF_3/BiOBr heterojunctions from microwave-assisted method and photocatalytic performances. *J. Hazard. Mater* 367, 304–315. doi: 10.1016/j.jhazmat.2018.12.060

Zhang, X., Ai, Z. H., Jia, F. L., and Zhang, L. Z. (2008). Generalized one-pot synthesis, characterization, and photocatalytic activity of hierarchical BiOX (X=Cl, Br, I) nanoplate microspheres. *J. Phys. Chem. C.*112, 747–753. doi: 10.1021/jp077471t

Zhang, Y. J., Thomas, A., Antonietti, M., and Wang, X. C. (2009). Activation of carbon nitride solids by protonation: morphology changes, enhanced ionic conductivity and photoconduction experiments. *J. Am. Chem. Soc.* 131, 50–51. doi: 10.1021/ja808329f

Zhou, J. W., Zhang, M., and Zhu, Y. (2014).Preparation of visible light-driven g-C_3N_4/ZnO hybrid photocatalyst via mechanochemistry. *Phys. Chem. Chem. Phys.* 16,17627–17633. doi: 10.1039/C4CP02061H

Zhu, L. F., He, C., Huang, Y. L., Chen, Z. H., Xia, D. H., Su, M. H., et al. (2012). Enhanced photocatalytic disinfection of *E. coli* 8099 using Ag/BiOI composite under visible light irradiation. *Sep. Purif. Technol.* 91, 59–66. doi: 10.1016/j.seppur.2011.10.026

Zou, Z. G., Ye, J. H.,Sayama, K., and Arakawa, H. (2001). Direct splitting of water under visible light irradiation with an oxide semiconductor photocatalyst. *Nature* 414, 625–627. doi: 10.1038/414625a

Conflict of Interest: The authors declare that the research was conducted in the absence of any commercial or financial relationships that could be construed as a potential conflict of interest.